STATISTICS, OPTIMIZATION AND INFORMATION COMPUTING
Stat., Optim. Inf. Comput., Vol. **12**, November 2024, pp 2000–2021.
Published online in International Academic Press (www.IAPress.org)

On the Geometric Pattern Transformation (GPT) Properties of Unidimensional Signals

Cristian Bonini [1,5], Marcos Maillot [1,5], Dino Otero [2], Andrea Rey [3], Ariel Amadio [2,*], Walter Legnani [4]

[1] *Research, Development, and Innovation in Electrical Energy Center, Universidad Tecnológica Nacional Facultad Regional General Pacheco, Av. Hipólito Yrigoyen 288, B1617, General Pacheco, Argentina*
[2] *Vehicle Research, Development, and Innovation Center, Universidad Tecnológica Nacional Facultad Regional General Pacheco, Av. Hipólito Yrigoyen 288, B1617, General Pacheco, Argentina*
[3] *Center of Research and Development in Applied Informatics, Universidad Nacional de Hurlingham, Tte. Manuel Origone 151, B1688, Villa Santos Tesei, Argentina*
[4] *Signal and Image Processing Center, Universidad Tecnológica Nacional Facultad Regional Buenos Aires, Av. Medrano 951, C1179, Buenos Aires, Argentina*
[5] *Department of Electrical Engineering , Universidad Tecnológica Nacional Facultad Regional General Pacheco, Av. Hipólito Yrigoyen 288, B1617, General Pacheco, Argentina*

Abstract The Geometric Pattern Transformation (GPT) has several advantages of use concerning contemporary algorithms that have been duly studied in previous research. With regard to some of its properties, four different but complementary aspects of the GPT are presented in this work. After a brief review of the GPT concept, how tied data are manifested in data sets is shown, to obtain a symmetric representation of the GPT, a linear transformation is performed that regularizes the geometric representation of the GPT and the theoretical relationship between the GPT and the phase-state representation of 1D signals is analyzed and formalized; then the study of the forbidden pattern is easily revealed, obtaining a strong relationship with the stable and unstable fixed points of the logistic equation. Finally, the characterization of colored noise and the application in real-world signals taken through experimental procedures are analyzed. With these results, in this work an advance in the potential applications of the GPT is proposed in an integral way in the processing and analysis of data series.

Keywords Phase Space, Tied Data, Noise Characterization, Forbidden Patterns, Fixed Point.

MSC 2020 subject classifications 94A12, 94A17

DOI: 10.19139/soic-2310-5070-1924

1. Introduction

To extend the field of applications and spread the use of the GPT [1], it is essential to establish properties that are of interest for application in the signal and data analysis community. In the present work some properties are developed that are related to repeated (tied) data, phase space, useful in the study of system dynamics, forbidden patterns [2, 3] and characterization of noise in acquired signals [4].

The detection and management of repeated values in data series is a topic of ongoing interest that can be treated in different ways. Employing the GPT in the present work, a new alternative is presented so that once detected, which is a fact that the GPT does in a very efficient way, they can be processed for its later application.

*Correspondence to: Ariel Amadio (Email: aamadio@docentes.frgp.utn.edu.ar). Vehicle Research, Development, and Innovation Center, Universidad Tecnológica Nacional Facultad Regional General Pacheco, Av. Hipólito Yrigoyen 288, B1617, General Pacheco, Argentina.

ISSN 2310-5070 (online) ISSN 2311-004X (print)

There is no need to go into detail regarding the usefulness of the analysis and study of the phase space that is reconstructed from a 1D signal [5]. Consequently, in the present work, the GPT and the phase space are found equivalents with a series of linear transformations developed to regularize and normalize the hexagon containing the GPT. With this consequent normalization, the GPT is independent of the signal amplitude, thus allowing one to compare signals that may have similar characteristics but different scales. Furthermore, transformations that bring the GPT into phase space were developed. The main advantage of linking the GPT with the phase space is that no parameter estimation or setting must be performed to obtain the phase space of a 1D signal, as is required by most algorithms developed in the existing literature [6].

For the case of forbidden patterns, an example in chaotic models with the logistics equation is shown not only numerically in the GPT but also analyzed analytically to explain the non-appearance of a given sequence of patterns in the previously indicated chaotic map. Although the phenomenon of forbidden patterns in chaotic discrete dynamical systems is a known fact, it has been shown that the GPT is a versatile graphical tool for their detection.

Closing the set of applications of the GPT, the characterization of colored and Gaussian noises is presented. Three examples are included to show the use in real world signals. In such a way is the case of the characterization of noise in ECG signal. In this particular case, Physionet signals corresponding to normal sinus rhythm [7] recording with low noise levels, a case of internal partial discharge in oil-impregnated presspan [8], and finally a white noise generated in a sound laboratory recorded using electronic devices. It should be pointed out that all the signals of the last section have been taken to characterize their respective noises without resorting to Fourier frequency analysis or any type of filter.

This work ends with the appropriate conclusions where, in addition to analyzing the results presented, a brief review of the limitations of GPT is included and its use in the framework of the signal processing workflow is succinctly presented.

2. Geometric pattern transformation

The GPT is a valid and recent alternative to traditional signal analysis methodologies based on ordinal patterns. Its advantages include the fact that it does not require the adjustment of any parameters, it can be used on signals whose length prevents other methodologies from being applied, the algorithm requires that the sampling frequency theorem must be accomplished, and it is computationally efficient. The motivation for its development was fundamentally related to the need to differentiate signals whose similarity made it impossible to distinguish them using other analytical methodologies [1].

Formally, the GPT is defined in terms of mathematical language, as a linear transformation $\mathcal{G} : \mathbb{R}^3 \to \mathbb{R}^2$ given by

$$\mathcal{G}(x, y, z) = (2z - y - x, z - x). \tag{1}$$

Given a times series $\{y_1, y_2, \ldots, y_N\}$, the function $\mathcal{G}$ can be applied to the elements formed by three consecutive observations in the series. In other words, for each $i = 1, 2, \ldots, N-2$ there exists a point $\mathcal{G}(y_i, y_{i+1}, y_{i+2})$. It was established in this proposal the existence of three lines that geometrically separate the cloud of these points in the six regions corresponding to the ordinal patterns described in Figure 1 and labeled as 123, 213, 312, 321, 231, and 132 (see [1] for details). Hereafter y_i for $i = 1, \ldots, N$ is reserved for the values of the signal to be considered, while the letter y without the corresponding sub-index refers to the variable of the vertical axis of the Cartesian plane $\mathbb{R}^2$, while x and z are reserved to their usual assignation.

From the expression 1, the first component represents the moment variation (ΔM) and the second component represents the state variation (ΔS). Thus, the image of $\mathcal{G}$ can be viewed in a plane named $\Delta M \times \Delta S$.

The application of the GPT does not require to fulfill any additional requirements as in the case of other algorithms used in signal processing methodologies. With the application of the GPT is not necessary to analyze the periodic or non-periodic characteristic of the signal as in the case of the Fourier analysis [9]. In the case of other transforms, for example wavelet transform, is necessary to select the basis of functions to be used and scales range or maximum level of decomposition selected [10].

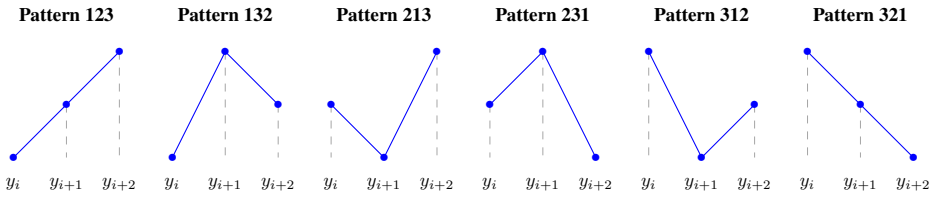

Figure 1. Ordinal patterns of three successive points.

For the case of signal analysis techniques in time domain, like as the correlation analysis or any of the usually statistical methods, the length of the data series imposes a significant limitation [10] which is absent with the use of the GPT.

Comparatively the GPT could be associated with signal processing techniques which apply diversity of permutation ordinal patterns methodologies, as well as the case of the permutation entropy [11] and its many variants [12]. To apply any methodology of the permutation patterns, it demands the selection of almost two parameters which requires a deep analyses of the particular application, usually known as the time delay embedding and the embedding dimension, see for details for example [13] and [14]. To apply the GPT is not necessary this selection.

In some way the GPT will be incorporated in the set of signal processing tools of symbolic dynamics (for more information can be consulted [15] and [16]), because it analyzes the sequence of the appearance of points in the signal, and locate these points in the above mentioned plane given by Eq.(1).

With respect to the use of informational tools like entropies, for example the Tsalis [17] or Renyi entropy [18] or many of the mostly applied complexities, the use of them requires the selection of parameters which have implications in the results, in such a way there are examples in [19] and [20], which is another advantage proper of the GPT algorithm that not is necessary to set up any additional parameter.

In other order, the application of the GPT do not demand any assumption about the nature of the signal, which is called agnostic to signal origin. Conceptual clarity, computational efficiency, easy of implementation and less limitations in computation with other signal analysis tools provide to the GPT algorithm a profile can be interesting to be explored in detail.

3. GPT and tied data

In this section, the projection of the tied data onto the GPT plane is analyzed. The tied data are defined as a pair of numbers with equally value in a given embedding vector (y_i, y_{i+1}, y_{i+2}). In signal processing, this can be found when a signal has two consecutive successive samples, or in a short period of time, with the same value. In the Figure 2 are defined regions where $L_1 : \Delta S = \Delta M$, $L_2 : \Delta S = \Delta M/2$ and $r : \Delta S = 0$. It is necessary to introduce the following notation: $L_j^{(+)}$ and $L_j^{(-)}$ that indicates the portion of the line L_j, for $j = 1, 2$, in the first and third quadrants respectively. Meanwhile, $r^{(+)}$ and $r^{(-)}$ denote the positive and negative horizontal semiaxes, respectively.

Going in detail about the concept of this separation, as a first step it is necessary to express ΔS as a function of ΔM using the following relation:

$$\Delta S = \Delta M - y_{i+2} + y_{i+1}. \tag{2}$$

Let's see the separation between the patterns:

$$132 \longleftrightarrow y_{i+1} > y_{i+2} > y_i \qquad \text{and} \qquad 123 \longleftrightarrow y_{i+2} > y_{i+1} > y_i.$$

It is clear that the condition $y_{i+2} > y_i$, or equivalently $\Delta S > 0$, is fulfilled by both patterns and that the passage from one pattern to the other one occurs when the relationship $y_{i+2} > y_{i+1}$ is inverted, which means that the

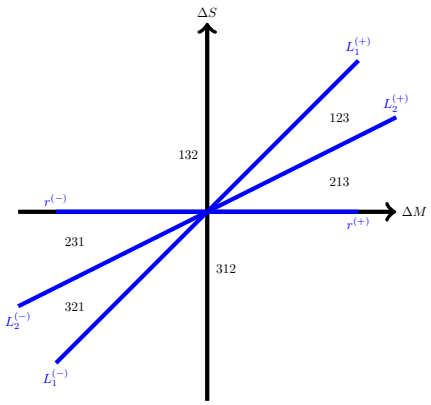

Figure 2. Ordinal pattern regions occupied by the GPT points.

condition of the change holds when $y_{i+2} = y_{i+1}$. Replacing in Eq. (2), $\Delta S = \Delta M$ which is precisely the half-line $L_1^{(+)}$ dividing the regions between patterns 123 and 132.

Analogously, it can be formulated for the following patterns:

$$123 \longleftrightarrow y_{i+2} > y_{i+1} > y_i \qquad \text{and} \qquad 213 \longleftrightarrow y_{i+2} > y_i > y_{i+1}.$$

The only reversed relationship occurs between y_{i+1} and y_i. Replacing in the expression (2) by the equality $y_{i+1} = y_i$, it can be seen that $\Delta S = \Delta M/2$. Thus, the transition between patterns 123 and 213 is described by the half-line $L_2^{(+)}$ since in this case $\Delta S < 0$ is also satisfied.

To analyze the transition between the patterns:

$$213 \longleftrightarrow y_{i+2} > y_i > y_{i+1} \qquad \text{and} \qquad 312 \longleftrightarrow y_i > y_{i+2} > y_{i+1},$$

it is noticed that the reversed relationship appears between y_{i+2} and y_i. The equality $y_{i+2} = y_i$ implies that $\Delta S = 0$. Since $\Delta M > 0$ for points that correspond to pattern 213, the transition between patterns 213 and 312 is represented by the half-line $r^{(+)}$.

The limits between the transitions of the other three pairs of adjacent patterns can be observed similarly. Table 1 summarizes the limits that define the possible pattern transitions in the presence of tied data, where the 3-tuple (y_i, y_{i+1}, y_{i+2}) in the first column represents three consecutive values in the signal. To the simplify notation, we identify each type of tied data with a label as shown in the second column of this table, where the upper case letter indicates the maximum value in the 3-tuple.

Table 1. Delimiters of pattern transition regions for tied data.

Tied data type	**Identification**	**Pattern transition**	**Delimiter**
(b, a, a) with $a > b$	bAA	$123 \longleftrightarrow 132$	$L_1^{(+)}$
(a, a, b) with $a < b$	aaB	$123 \longleftrightarrow 213$	$L_2^{(+)}$
(a, b, a) with $a > b$	AbA	$213 \longleftrightarrow 312$	$r^{(+)}$
(b, a, a) with $a < b$	Baa	$312 \longleftrightarrow 321$	$L_1^{(-)}$
(a, a, b) with $a > b$	AAb	$231 \longleftrightarrow 321$	$L_2^{(-)}$
(a, b, a) with $a < b$	aBa	$132 \longleftrightarrow 213$	$r^{(-)}$
(a, a, a)	aaa	undefined	0

In this way the GPT plane has the ability to project the tie data of the signal in these semi-straight lines. This means that a high density of point near these semi-straights lines indicates similar values between a pair of samples in the embedding vector.

4. Regularization of GPT and phase space

This Section is devoted to the description and deduction of the linear transformations which are going to be used to prove that the phase space is represented in terms of the GPT.

The wide range of studies that have capitalized on the usefulness of the phase space representation is very huge. In fact, the number of works on the subject is hard to enumerate. The areas in which the concept of phase space was applied have continuously grown since the last quarter of the XX century.

The works that use phase space cover a wide range of disciplines ranging from classical physics to quantum physics, and many other disciplines (see just for a minimum example [21, 22, 23, 24, 25]). On the other side, it is frequent to find a great diversity of experimental and theoretical studies, developed both in the time and frequency domains and both simultaneously as in the case of wavelets concerning the concept of phase space.

Let a 1D signal that accomplishes the Nyquist frequency criteria, in the sense that the sampling frequency is adequate, from the 2D constituted by $\Delta M \times \Delta S$ is possible to obtain the corresponding representation of the above-mentioned signal in the corresponding phase space.

Hexagon regularization. When the GPT is applied to a uniform random signal with values in the interval $[0, b]$, with $b > 0$, the resulting points are located within the hexagon shown in Figure 3 (left) (see [1] for details). The vertices are $V_1 = (2b, b)$, $V_2 = (b, b)$, $V_3 = (-b, 0)$, $V_4 = (-2b, -b)$, $V_5 = (-b, -b)$, and $V_6 = (b, 0)$. The interest is focused on transforming this hexagon into a regular one inscribed in the unitary circumference as shown in Figure 3 (right). For that reason, were defined the points $W_1 = (1/2, \sqrt{3}/2)$ and $W_2 = (-1/2, \sqrt{3}/2)$ to find that transformation called $\mathcal{R}$. Since $B = \{V_1, V_2\}$ is a basis of $\mathbb{R}^2$, the Fundamental Theorem of Linear Transformations can be applied to obtain the expression of the linear function $\mathcal{R} : \mathbb{R}^2 \to \mathbb{R}^2$ such that $\mathcal{R}(V_1) = W_1$ and $\mathcal{R}(V_2) = W_2$.

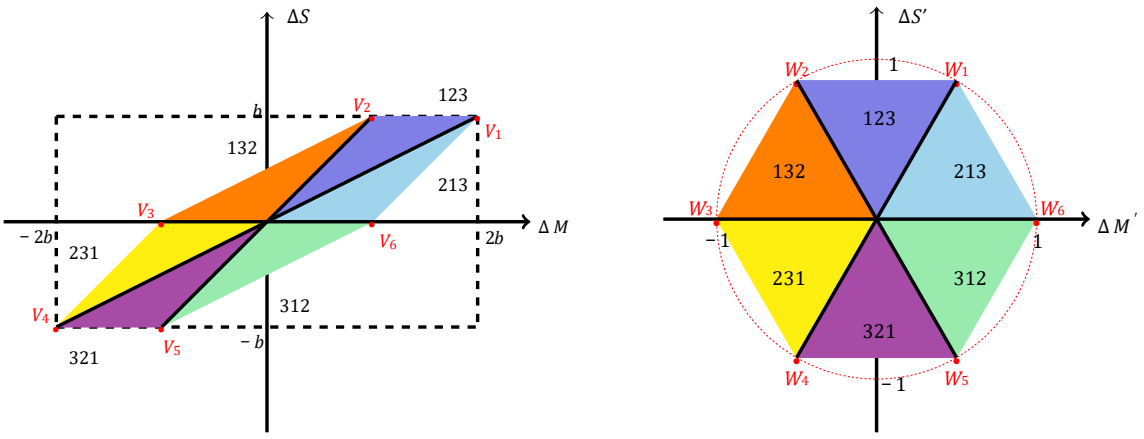

Figure 3. Original (left) and regularized (right) hexagons defined by the GPT applied to a uniform random signal in $[0, b]$.

First, the coordinates in the basis B of a generic point $(x, y) \in \mathbb{R}^2$ are found; i.e. $[(x, y)]_B = (\alpha, \beta)$, where $(x, y) = \alpha(2b, b) + \beta(b, b)$. A simple computation proves that $\alpha = (x - y)/b$ and $\beta = (2y - x)/b$.

Hence,

$$\begin{aligned}\mathcal{R}(x, y) &= \mathcal{R}[\alpha(2b, b) + \beta(b, b)] = \alpha\mathcal{R}(2b, b) + \beta\mathcal{R}(b, b) = \alpha\mathcal{R}(V_1) + \beta\mathcal{R}(V_2) = \alpha W_1 + \beta W_2 \\ &= \frac{x - y}{b}\left(\frac{1}{2}, \frac{\sqrt{3}}{2}\right) + \frac{2y - x}{b}\left(-\frac{1}{2}, \frac{\sqrt{3}}{2}\right) = \left(\frac{1}{b}x - \frac{3}{2b}y, \frac{\sqrt{3}}{2b}y\right). \end{aligned} \tag{3}$$

In other words, if $\mathcal{R}(x, y) = (x', y')$, then

$$\begin{cases} x' &= \dfrac{1}{b}x - \dfrac{3}{2b}y, \\ \\ y' &= \dfrac{\sqrt{3}}{2b}y. \end{cases} \tag{4}$$

Applying the expressions (4) to the rest of the vertices, the following results can be verified:

$$\begin{aligned} &\mathcal{R}(V_3) = \mathcal{R}(-b, 0) = (-1, 0) = W_3, \\ &\mathcal{R}(V_4) = \mathcal{R}(-2b, -b) = (-1/2, -\sqrt{3}/2) = W_4, \\ &\mathcal{R}(V_5) = \mathcal{R}(-b, -b) = (1/2, -\sqrt{3}/2) = W_5, \\ &\mathcal{R}(V_6) = \mathcal{R}(b, 0) = (1, 0) = W_6. \end{aligned}$$

It means that $\mathcal{R}$ transforms the hexagon given by the GPT to a regular hexagon inscribed in the unitary circumference.

In [1], it was determined that the vertices of the hexagon were defined by the signal values. Now, this result can be used to normalize any signal within the GPT. For example, for a random signal of 10,000 samples to holds all types of patterns and its variants, the irregular hexagon is filled, and the same happens with the normalized hexagon (see Figure 8 (c)).

Phase space. Given a twice differentiable function $w = f(t)$ with support $\mathbb{R}$, the phase space is defined by the terns $(w, w', w'') \in \mathbb{R}^3$. The phase space are obtained by the orthogonal projections $(w, w', 0)$, $(w, 0, w'')$ and $(0, w', w'')$. In the following lines, the focus point is on the last projection.

Let $\{w_i = f(t_i) : i = 1, 2, \ldots, N\}$. Then, for $h > 0$, the derivatives can be approximated by the following expressions:

$$f'(t_i) = w_i' \cong \frac{w_{i+1} - w_{i-1}}{2h}, \tag{5}$$

$$f''(t_i) = w_i'' \cong \frac{w_{i+1} - 2w_i + w_{i-1}}{h^2}. \tag{6}$$

Thus, two linear transformations $\mathcal{P}_h, \mathcal{P}_h^* : \mathbb{R}^3 \to \mathbb{R}^2$ can be defined as:

$$\mathcal{P}_h(x, y, z) = \left(\frac{z - x}{2h}, \frac{z - 2y + x}{h^2}\right), \tag{7}$$

$$\mathcal{P}_h^*(x, y, z) = \left(\frac{z - 2y + x}{h^2}, \frac{z - x}{2h}\right). \tag{8}$$

If $\mathcal{T} : \mathbb{R}^2 \to \mathbb{R}^2$ is the linear transformation defined by $\mathcal{T}(x, y) = (y, x)$, then it is clear that $\mathcal{P}_h = \mathcal{T} \circ \mathcal{P}_h^*$. In addition, $\mathcal{P}_h(w_{i-1}, w_i, w_{i+1})$ coincides with the pair whose components are those of expressions (5) and (6). Hence, the phase space $(0, w', w'')$ is isomorphic to $\text{Im}(\mathcal{P}_h)$, which is also isomorphic to $\text{Im}(\mathcal{P}_h^*)$, where Im denotes the image of a function.

Table 2. Matrices associated with linear transformations.

Transformation	Matrix
$\mathcal{G}$	$M(\mathcal{G}) = \begin{pmatrix} -1 & -1 & 2 \\ -1 & 0 & 1 \end{pmatrix}$
$\mathcal{P}_h$	$M(\mathcal{P}_h) = \begin{pmatrix} -(2h)^{-1} & 0 & (2h)^{-1} \\ h^{-2} & -2h^{-2} & h^{-2} \end{pmatrix}$
$\mathcal{R}$	$M(\mathcal{R}) = \begin{pmatrix} b^{-1} & -3(2b)^{-1} \\ 0 & \sqrt{3}(2b)^{-1} \end{pmatrix}$
$\mathcal{T}$	$M(\mathcal{T}) = \begin{pmatrix} 0 & 1 \\ 1 & 0 \end{pmatrix}$
$\mathcal{S}$	$M(\mathcal{S}) = \begin{pmatrix} 2b & 0 \\ 0 & 3^{-1}b\sqrt{3} \end{pmatrix}$
$\mathcal{S}_h^*$	$M(\mathcal{S}_h) = \begin{pmatrix} h^{-2} & 0 \\ 0 & h^{-1} \end{pmatrix}$

Scalar transformation. Two scale transformations are necessary to relate the GPT with the phase space, another corresponding to the hexagon regularization and one considering the increment h in the numeric derivatives. Let $\mathcal{S}, \mathcal{S}_h : \mathbb{R}^2 \to \mathbb{R}^2$ be two functions defined by:

$$\mathcal{S}(x, y) = \left(2bx, \frac{b\sqrt{3}}{3}y\right), \tag{9}$$

$$\mathcal{S}_h^*(x, y) = \left(\frac{x}{h^2}, \frac{y}{h}\right). \tag{10}$$

The matrix notation in the canonical basis of $\mathbb{R}^2$ and $\mathbb{R}^3$ of the previous transformations are shown in Table 2.

A direct computation proves that

$$M(\mathcal{P}_h) = M(\mathcal{T}) \cdot M(\mathcal{S}_h) \cdot M(\mathcal{S}) \cdot M(\mathcal{R}) \cdot M(\mathcal{G}), \tag{11}$$

and, hence,

$$\mathcal{P}_h = \mathcal{T} \circ \mathcal{S}_h \circ \mathcal{S} \circ \mathcal{R} \circ \mathcal{G}. \tag{12}$$

Thus, it has been proved that the phase space is the GPT composed by a rotation, a scaling, and a permutation of coordinates.

In the case of a discrete signal which is a data series consisting of a sequence of quantities disregarding the specific value of the time between data points, the value of the parameter h can be assumed as one.

5. GPT and forbidden patterns

For the case of deterministic chaotic 1D maps not all the possible ordinal patterns can be effectively materialized into orbits as was presented in [2, 26, 27, 28]. These patterns can be interpreted as forbidden. In such a way the existence of these forbidden ordinal patterns becomes a persistent property that can be understood as an emerging dynamic characteristic of some systems. The concept of a forbidden pattern has a different meaning than the concept of the missing pattern since the last one is reserved for the case in which the absence could be done

by the signal length. In this context, for a fixed embedding dimension, the number of unobserved or forbidden patterns of a time series is independent of its length [29]. In the case of stochastic time series could also appear forbidden patterns [30], but in other many classes of noises, it can be numerically verified that no forbidden patterns emerge [29]. A detailed analysis of the forbidden patterns paradigm and its study with informational measures can be found in [3].

Forbidden patterns can be clearly and quickly identified using the GPT. For example, Figure 4 shows the absence of pattern 321 when the GPT is applied to a signal generated by the logistic equation given by

$$y_{i+1} = ry_i(1 - y_i), \tag{13}$$

for all $i \in \mathbb{Z}^+$, $y_1 \in (0, 1)$ and with parameter $r \in \mathbb{R}$ ranging from 2 to 4. The reason for this property can be proved easily as follows. Let $y_1, y_2, \ldots, y_N$ be a signal generated by the recursive equation (13). Suppose that, without ties, the pattern 321 appears in the signal, then there exists $j \in \mathbb{Z}^+$ such that $y_j > y_{j+1} > y_{j+2}$. In particular,

$$0 < y_j - y_{j+1} = y_j - ry_j(1 - y_j) = y_j(1 - r + ry_j). \tag{14}$$

Since $y_j > 0$, it holds that $y_j > (r - 1)/r = 1 - 1/r$. Thus, there exists $\varepsilon \in \mathbb{R}_{>0}$ such that

$$y_j = 1 - \frac{1}{r} + \varepsilon. \tag{15}$$

On the other hand, replacing (15) in (13), then

$$y_{j+1} = r\left(1 - \frac{1}{r} + \varepsilon\right)\left[1 - \left(1 - \frac{1}{r} + \varepsilon\right)\right] = 1 - \frac{1}{r} + \varepsilon(2 - r - r\varepsilon). \tag{16}$$

Analogously, it can be deduced that $y_{j+1} > 1 - 1/r$. Hence, by (16) and since $\varepsilon > 0$, $0 < 2 - r - r\varepsilon < 2 - r$, which implies that $r < 2$ contradicting the exposed context.

This result is in agreement with the numerical simulation exhibited in Figure 4 where no points are projected onto the 321 region. Although in the algebraic demonstration, the absence of the pattern 321 in the signal defined by the logistic map is due to the type of function that generates it, the use of the GPT quickly revealed the forbidden for $2 < r < 4$. Another additional important result, concerning the condition given by $y_i = 1 - 1/r$ should be highlighted. This case constitutes a stable fixed point for $2 < r < 3$, and an unstable point for $3 \leq r \leq 4$. Despite the existence of the unstable fixed point already known in [31], this close connection with the absence of a pattern is a new result. It is possible to speculate that the forbidden patterns may be due to obvious characteristics of the signal or, as in this case, to the existence of an associated instability.

Several works have analyzed the absence of patterns as was presented above in this section. In the case of the logistic map, there is another interesting forbidden pattern under certain conditions. The absence of pattern 123 when the GPT is applied to the signal generated by the logistic equation is strongly linked with the existence of the fixed point.

Starting from the expression (13), with the parameter r ranging from 2 to 4 is to possible study analytically the absence of the pattern 123. Analogous to (15), *mutatis mutandi* in this case:

$$y_j = 1 - \frac{1}{r} - \varepsilon,\ \varepsilon > 0, \tag{17}$$

and then

$$y_{j+1} = r\left(1 - \frac{1}{r} - \varepsilon\right)\left[1 - \left(1 - \frac{1}{r} - \varepsilon\right)\right] = 1 - \frac{1}{r} + \varepsilon(r - r\varepsilon - 2). \tag{18}$$

The presence of the pattern 123 implies the following condition:

$$r < \frac{2}{1 - \varepsilon}, \tag{19}$$

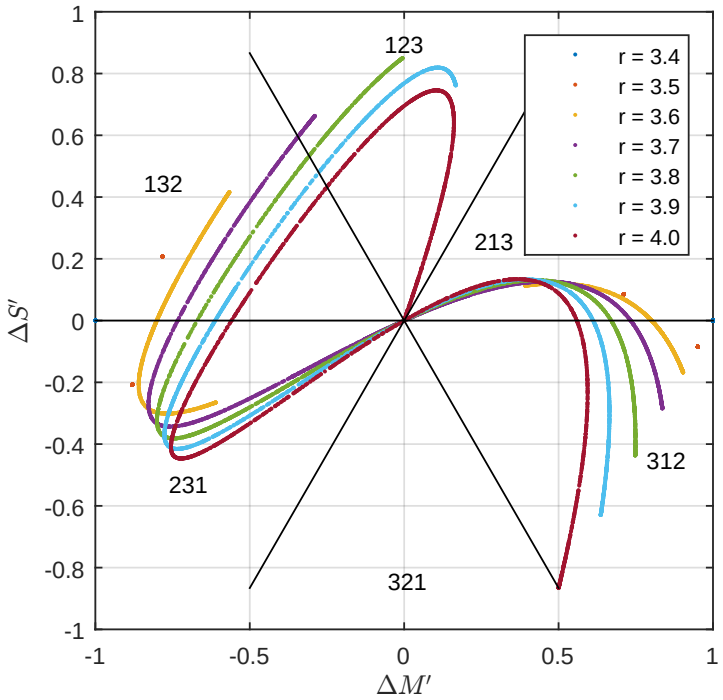

Figure 4. Patterns for signal from the logistic equation after the transient phase for different r parameter values. Pattern 321 is forbidden.

where $\varepsilon < 1$. This result implies that the pattern exists for any value of r, taking ε appropriately. In reality, it can be verified that the appearance occurs in the first iterations of the transitory phase. However, for $r < 3.67857$, the pattern appears beyond the transient phase. This is shown in Figure 4 for a range of the parameter r from 3.4 to 4. At $r = 3.4$ (dark blue curve) only 2 points are mapped onto GPT, as the logistic signal is varying only between 2 values (logistics is in 2-periods oscillation). For $r = 3.5$ (light red) the signal takes 4 values (logistics is on 4-period oscillation) and 4 symbols are allowed to express; each of them with the same coordinate. In the case of $r = 3.6$ (ocher curve) the logistics has reached a chaotic regime, thus allowing the presence of the same symbols with a wider range of possible values. Nevertheless, in any of the last cases analyzed, the 123 patterns is presented. Only with $r > 3.67857$ (i.e $r = 3.7$, violet curve) the 123 pattern is presented beyond the transient phase. At this value of r, the two chaotic branches meet and the area covered by chaos allows the condition (19) to be satisfied beyond the transient phase. Having clarified the condition for which pattern 123 is observed, we can find a general condition for y_i. Setting the condition (20) for $\varepsilon > 1 - 2/r$. Substituting in (18), the condition is still satisfied for $r > 2$:

$$y_i < 1 - \frac{1}{r} - 1 + \frac{2}{r}, \tag{20}$$

which implies that $y_i < 1/r$. In other words, the condition for the appearance of pattern 123 corresponds to the iteration of values lower than a hyperbola starting at 0.50 and ending at 0.25 for r = 4. Finally, it is possible to combine the condition for the presence of pattern 321 and the condition for the presence of pattern 123. For pattern 123 $y_i < 1 - 1/r$ or $y_i > 1/r$, and for pattern 321 $y_i > 1 - 1/r$ or $y_i < 1/r$, values of the fixed point ($y_i = 1 - \frac{1}{r}$ or $y_i = \frac{1}{r}$) are outside this conditions in such a way that both conditions converge to the same fixed point.

6. GPT and Analysis of Signal Noise

6.1. Characterization of colored and Gaussian noises

The characterization and treatment of noise has had an enormous importance in signal processing since the origin of telegraph communications. Nowadays, it can be said that communications [32], biomedical applications [33] and [34], and various uses in all types of industrial devices are demanding tools that contribute to the management of the different types of noise in the respective signals [35]. Therefore, characterizing different types of noise is of continuing interest in the signal and time series processing community since they can be used to predict events as in the case of geophysical analysis (see for example [35] and [36] and interior references).

This subsection is dedicated to show how the GPT applied to colored noises can discriminate them in a single and direct way processing the data series only in the time domain, without applying traditional signal processing techniques like filtering, filter banks, any kind of transform, or the well known and precise Fourier analysis.

A set of different colored noises signals of 10,000 points was generated following the work of Zhivomirov [37]. The signals vs. samples are showed in Figures 5 (a) to 10 (a), meanwhile from Figures 5 (b) to 10 (b) are presented their perspectives absolutes values of the Fast Fourier Transforms (FFTs), and from Figures 5 (c) to 10 (c) are exhibited the corresponding results after applied the GPT.

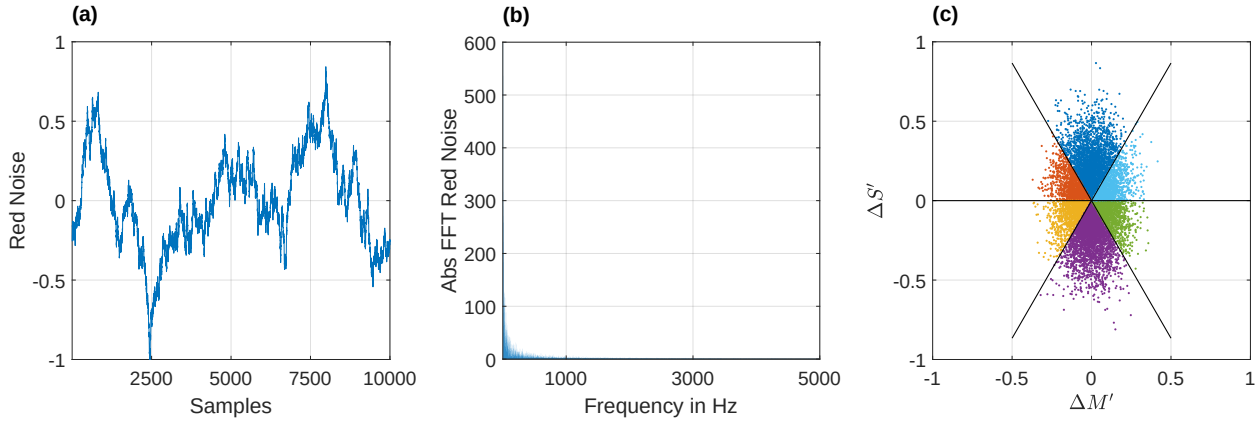

Figure 5. Red Noise: (a) signal vs. samples, (b) absolute value of the FFT of signal in (a), c) GPT of the signal showed in (a).

It is remarkable that the distribution of points provided by the GPT changes as the structure of the noise changes, showing different distributions in occupancy of the corresponding regions in the hexagon. That is, in the case of red noise (Figure 5 (c)) it results in an elliptical distribution elongated in the vertical direction, whose eccentricity begins to decrease in the case of pink noise (Figure 6 (c)). In the case of Gaussian noise as can see in Figure 7 (c) the cloud of points loss its eccentricity at all and concentrates more on the origin and for the case of white noise (Figure 8 (c)) becomes very uniform occupying all the regions of the hexagon. Blue noise begins to manifest an ellipse-shaped cloud points elongated in the horizontal direction see (Figure 9 (c)) that ends up being even more accentuated in the case of violet noise (Figure 10 (c))

To quantify the results described in the previous paragraph, some values were computed from the GPT plane and are shown in the table 3, where the first column corresponds to the noise denomination; the second contains the

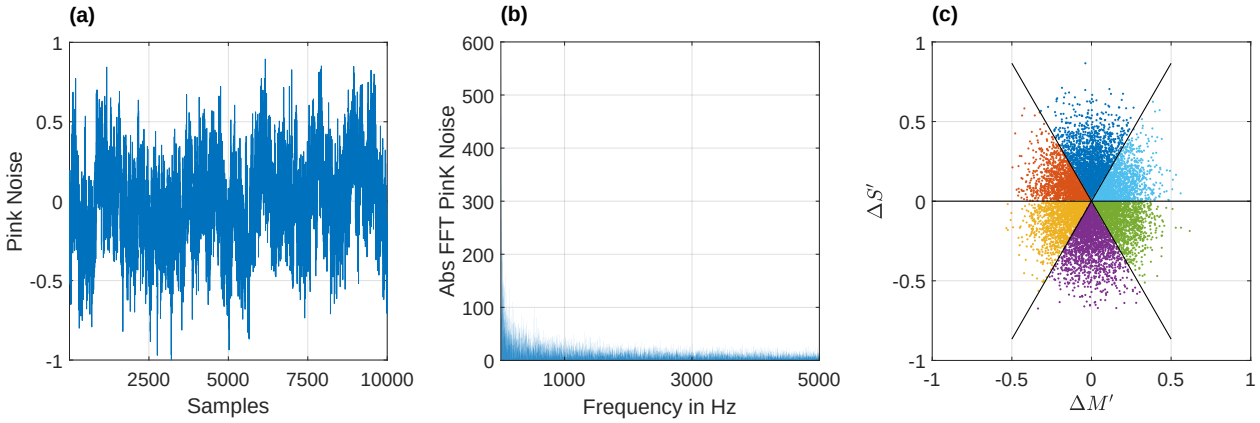

Figure 6. Pink Noise: (a) signal vs. samples, (b) absolute value of the FFT of signal in (a), (c) GPT of the signal showed in (a).

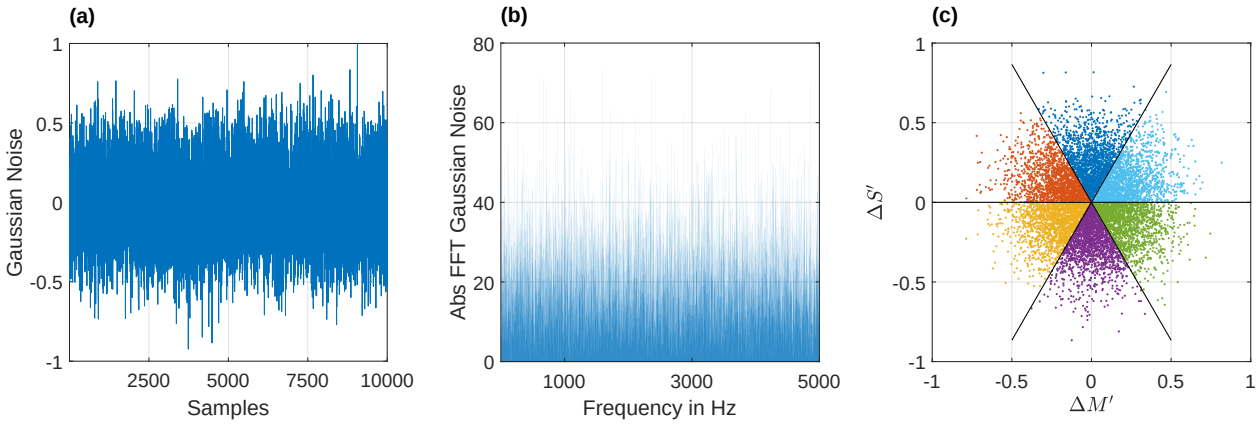

Figure 7. Gaussian Noise: (a) signal vs. samples, (b) absolute value of the FFT of signal in (a), (c) GPT of the signal showed in (a).

values of the eccentricity parameter ϵ computed applying expression (21) on each cloud of points resulting from the application of the GPT. Columns three through eight contain the normalized percentage of points resulting from the GPT that are counted in each sector of the GPT, which are labeled according Figure 1.

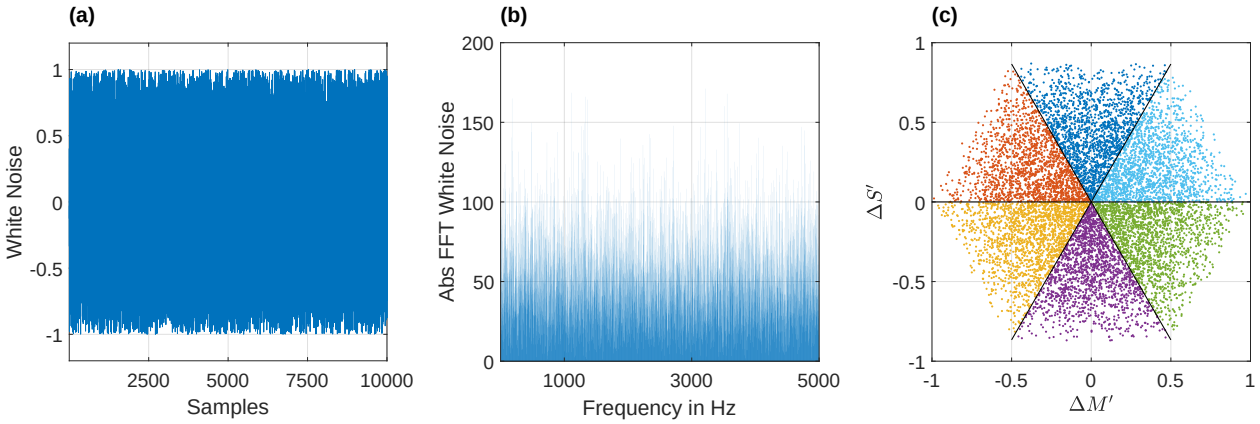

Figure 8. White Noise: (a) signal vs. samples, (b) absolute value of the FFT of signal in (a), (c) GPT of the signal showed in (a).

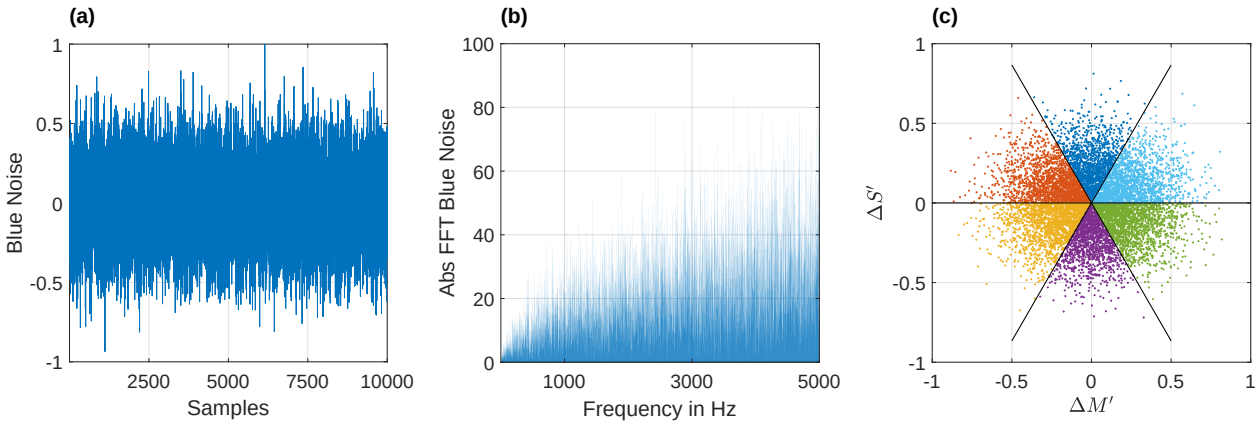

Figure 9. Blue Noise: (a) signal vs. samples, (b) absolute value of the FFT form of signal in (a), (c) GPT of the signal showed in (a).

$$\epsilon := \begin{cases} +\sqrt{1-(\frac{\sigma_{\Delta S'}}{\sigma_{\Delta M'}})^2} & \text{if} \quad \sigma_{\Delta S'} < \sigma_{\Delta M'} \\ \\ -\sqrt{1-(\frac{\sigma_{\Delta M'}}{\sigma_{\Delta S'}})^2} & \text{if} \quad \sigma_{\Delta S'} > \sigma_{\Delta M'} \end{cases}, \tag{21}$$

The eccentricity ϵ is proposed to describe the distribution of the GPT points from the noise signal. It measures the elongation of the ellipse that concentrate distribution of the points in the vertical or horizontal axis and is based

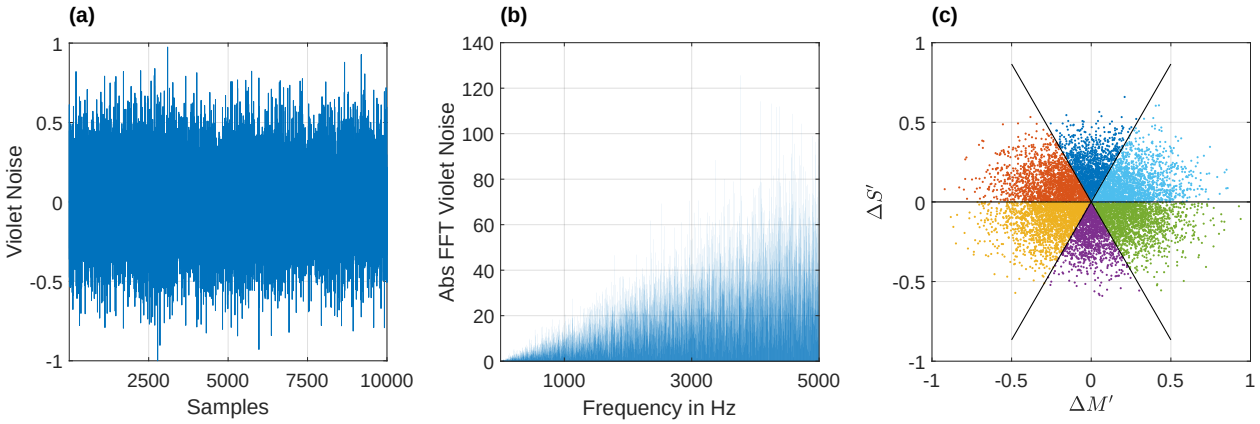

Figure 10. Violet Noise: (a) signal vs. samples, (b) absolute value of the FFT of signal in (a), (c) GPT of the signal showed in (a).

in the eccentricity of an ellipse, but in this case, the horizontal or vertical elongations are taken in consideration. It can be obtained with the expression (21),

From Table 3, there is another important result about the amount of information provided by the proposed methodology. The degree of uncertainty of a signal or time series can be estimated by the calculation of its entropy, in the case of the present work was selected the Shannon normalized entropy (S) given by:

$$S = - \frac{\sum_{i=1}^{6} p_i \cdot log(p_i)}{log(6)}, \tag{22}$$

where the index i runs form 1 to 6 which is the number of sectors of the hexagon of the GPT, and p_i is the probability estimated by the normalized percentage of occupancy of the cloud points in each sector of the hexagon.

The values of the column two shown in table 3, brings the possibility to characterize different noises under analysis, while columns three to eight provide information about the distribution of points in the different groupings resulting from the GPT calculation in the different types of noises, contributing to a complementary characterization. Not only the GPT shows the structure of the noise, but also the occupancy of sectors in the hexagon shows the contribution of each pattern.

Concluding the preliminary analysis of the results of table 3, it should be noted that with the chosen ordering for the colored noises the variation of the occupancy of each region in the hexagon varies in a monotonic way from the red to violet noise. Meanwhile the ϵ starts with a positive value for the red noise to finishing with a negative one for the violet noise. For the other noises the variation of ϵ is in descending order following the deformation of the point cloud from a ellipse with major axis in the vertical, with positive values of ϵ including the Gaussian, to the major axis parallel to the horizontal axis, with negative values of this parameter.

For a better analysis of the results obtained with the expressions (21) and (22) the results are represented in Figure 11. In the graphical inspection of the Figure 11 (a) can be observed the monotonic behaviour of the eccentricity of the cloud points obtained for the colored and Gaussian noises. In Figure 11 (b) is exhibited the variation of the normalized Shannon entropy for the different noises analyzed. The maximum values correspond to the white and Gaussian noise as is spectated. The rate of the occupancy of each region in the regions constructed from the GPT can be see in the Figure 11 (c) which contributes to understand how the proposed methodology gives a complementary characterization for every studied noise.

Noise	ϵ	123	132	231	321	312	213
Red	+0.8682	0.2724	0.1109	0.1158	0.2743	0.1139	0.1127
Pink	+0.6469	0.1988	0.1492	0.1462	0.2105	0.1388	0.1565
Gaussian	+0.1787	0.1691	0.1618	0.1701	0.1672	0.1654	0.1664
White	-0.1497	0.1668	0.1647	0.1716	0.1604	0.1697	0.1668
Blue	-0.6148	0.1381	0.1823	0.1817	0.1339	0.1846	0.1794
Violet	-0.7306	0.1205	0.1862	0.1925	0.1221	0.1892	0.1895

Table 3. The values in the six columns on the right correspond to the fraction of GPTs computations that occupied in each pattern by color noise, they are normalized in each row. The eccentricity ϵ is computed according the expression 21 .

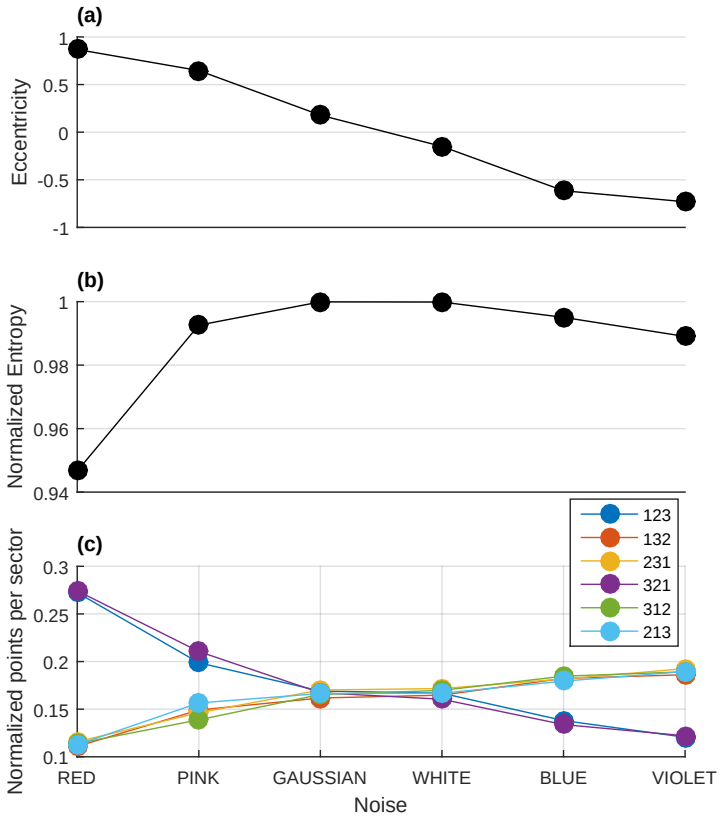

Figure 11. Graphical results of the GPT for the noises analysed: (a) Eccentricity for every noise, (b) Entropy of the different noises computed from 22, (c) Normalized percentage of occupancy of each sector of the regions of the GPT for the different noises corresponding to every pattern.

6.2. Examples of noise analysis in real world signals

This subsection is devoted to show real life applications of noise signal characterization applying the GPT.

6.2.1. Normal Sinus Rhythm Electrocardiogram The following case study is an electrocardiogram (ECG) of a subject with a normal recording taken from the Physionet database (normal sinus database [38]), see Figure 12 (left), analyzed using wavelet transform [39]. The main advantage of using wavelets is to localize the features of the signal at different scales, preserving important signal features while removing noise. In this way, the wavelet

transform concentrates signal features in a few large-magnitude wavelet coefficients. The wavelet coefficients that have small values can be associated with noise and can be discarded, in such a way that disregarding those coefficients does not affect the main signal shape [40]. Finally, after selecting the threshold coefficients to be retained, the signal can be reconstructed through the inverse wavelet transform in a well-known way.

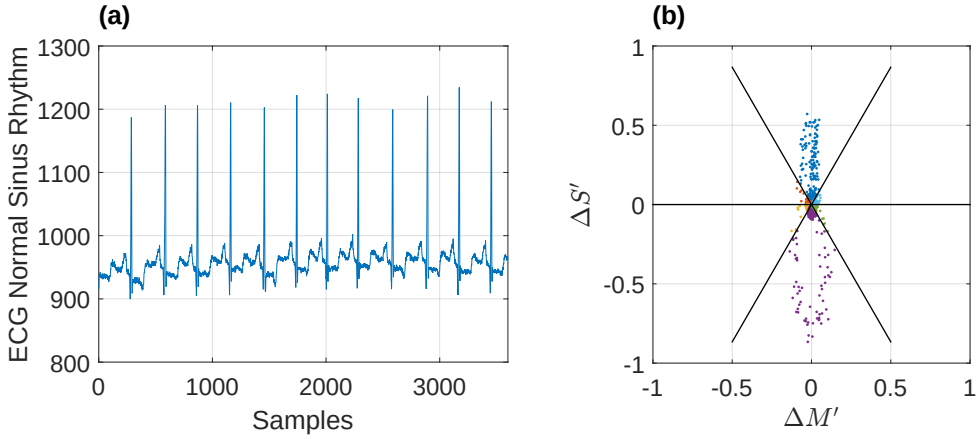

Figure 12. (a) ECG signal, (b) GPT of ECG.

The denoising made by wavelet Daubechies base of order 10, at level 5, and soft threshold [39] is presented in detail in Figure 14 (left), where the original and denoised signals are compared. The total residue or noise found by this method is plotted in Figure 13 (left).

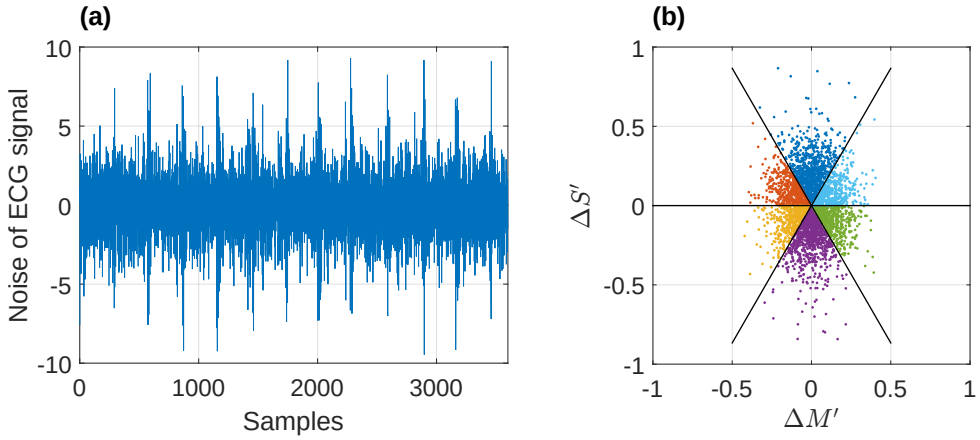

Figure 13. (a) ECG noise, (b) GPT of the ECG noise.

Figure 12 (right) shows the distribution of points of the application of GPT to the ECG normal sinus record being processed. The shape described in the plane $\Delta M' \times \Delta S'$ suggests that the signal under analysis has a strong periodic behavior, with an increase in the density of points corresponding to ascending 123 and descending 321 pattern sequences.

The presence of noise in the measured signals is observed in the area near the origin of the plane $\Delta M' \times \Delta S'$, for the signal under analysis. The amplitude of the cloud points at the origin is in direct relation to the amount of noise contained in the signal. Both, the horizontal and vertical amplitude of the cloud points characterizing the noise reflects the intensity of the noise in the signal. The use of the normalized GPT contributes to analyzing the effect of the noise and permits comparison with other signals independently of the amplitude of each one.

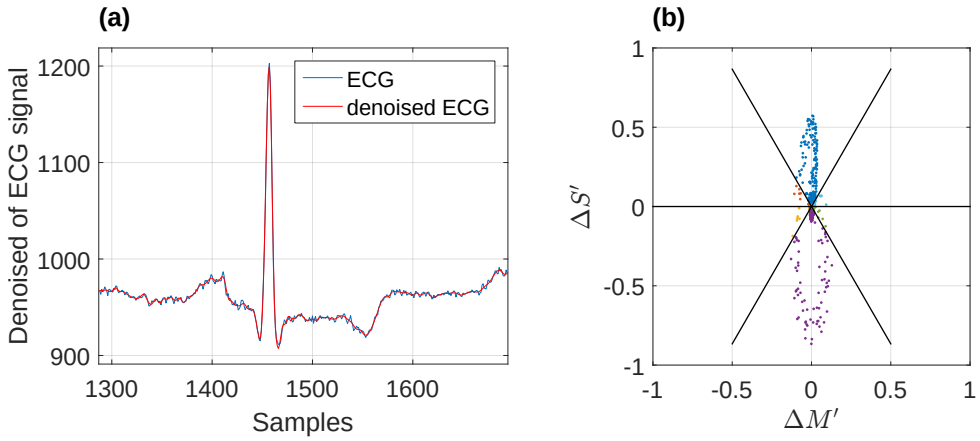

Figure 14. (a) Original and denoised ECG signal, (b) GPT of the denoised ECG.

After a light analysis of Figures 5 (c) to 10 (c) for the different type of colored noise and comparing with the GPT of the noise founded in the ECG signal (see Figure 13 (right), the characteristic distribution of points given by the GPT can be associated with an noise of pink type, where the points are concentrated around the origin of the plane $\Delta M' \times \Delta S'$ with a light elongation in the vertical direction. These observations can be sustained by the numerical results founded in table 3 for the colored noise and in table 4 for the real noise cases studied in this subsection.

The absolute value of the frequency spectrum of the noise found in the ECG signal is plotted in Figure 15. The presence of a tone in 60Hz and its harmonics of 120Hz and sub-harmonic in 30Hz is due to noise injected by the power line. This produces a increase in 123 and 321 pattern that elongates the cloud of point in the vertical axis. In addition, the distribution of the spectrum shifted to low frequency corresponds to noise of red to pink type. A superposition of the original ECG signal and the denoised version of it can be see in Figure 14 (a). Finishing the ECG example, the GPT of the denoised signal is presented in Figure 14 (b), where a remarkable reduction of points near the origin is observable indicating the reduction of the presence noise.

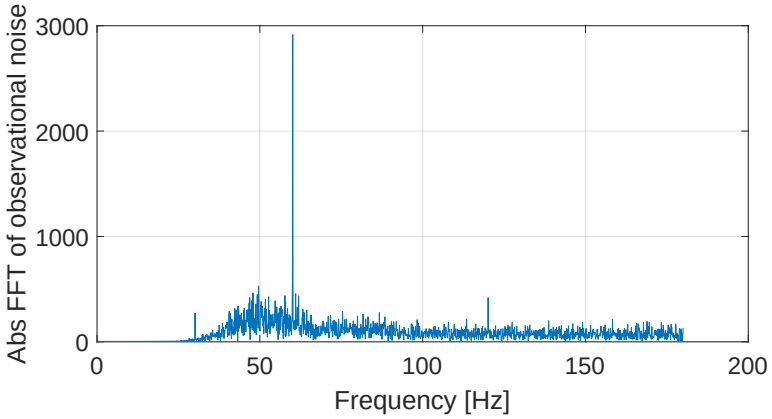

Figure 15. Module of FFT spectrum of noise of ECG signal.

6.2.2. Partial Discharge A partial discharge (PD) is a dielectric breakdown phenomenon that occurs within a insulating material due to the loss of symmetry in the distribution of electric field lines [41]. In the presence of the gas inclusions and/or impurities inside the material, the electric field converges and it intensifies locally in these

areas, causing the phenomenon in the form of small electric arcs which deteriorate the insulating medium. In this example, the noise presented in an internal PD pulse in oil-impregnated paper was characterized. The PD pulse was obtained in the laboratory under controlled conditions [8], [42].

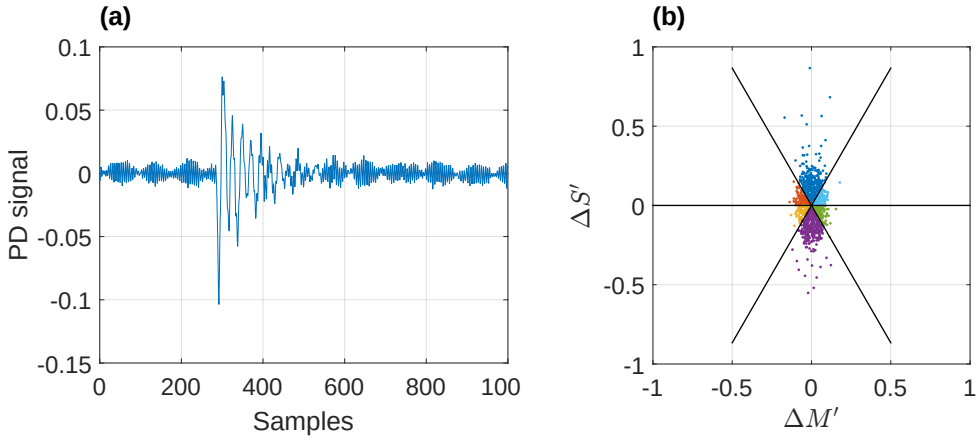

Figure 16. (a) Partial Discharge pulse, (b) GPT of the Partial Discharge pulse.

In Figures 16 (a) and (b), a raw DP pulse and its corresponding projection in the GPT transformed plane are presented. From the GPT plane, a main cloud with vertical orientation (positive eccentricity) can be distinguished; this us due to the high noise level contaminating the signal, an undesirable characteristic inherent to signal acquisition processes. The noise was separated from the signal using Wavelets, specifically a Daubechies of order 10, and a decomposition of level 2 was made. The detail levels d1 and d2 were separated to subsequently reconstruct the signal and calculate its GPT. The noise signal can be seen in Figure 17 (a), while its GPT transformation is shown in Figure 17 (b). In the latter, it can be observed that the distribution of points in the transformed plane and its eccentricity of 0.9090, calculated with expression (21), correspond to the characteristics of red noise, typical of the measurement process. See Table 3 and Figure 5 (c).

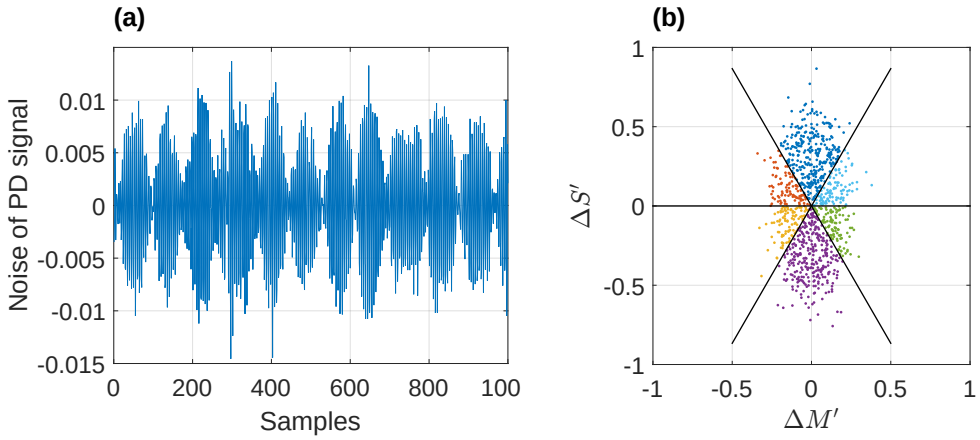

Figure 17. (a) Partial Discharge noise, (b) GPT of the Partial Discharge noise.

The absolute value of the frequency spectrum is presented en Figure 18 where two main components are presented in the range of 100MHz, which it is due to the test configuration.

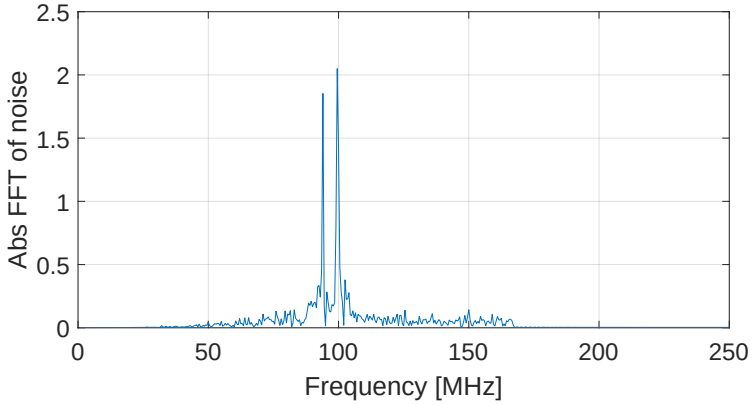

Figure 18. Module of FFT spectrum of noise of PD signal.

Finally, in Figure 19 (a) and (b), the filtered PD pulse and its corresponding GPT transformation are presented. It can be seen that given the structural characteristics of the signal without noise, where patterns 123 and 321 predominate, they form such a singular point distribution in the transformed plane.

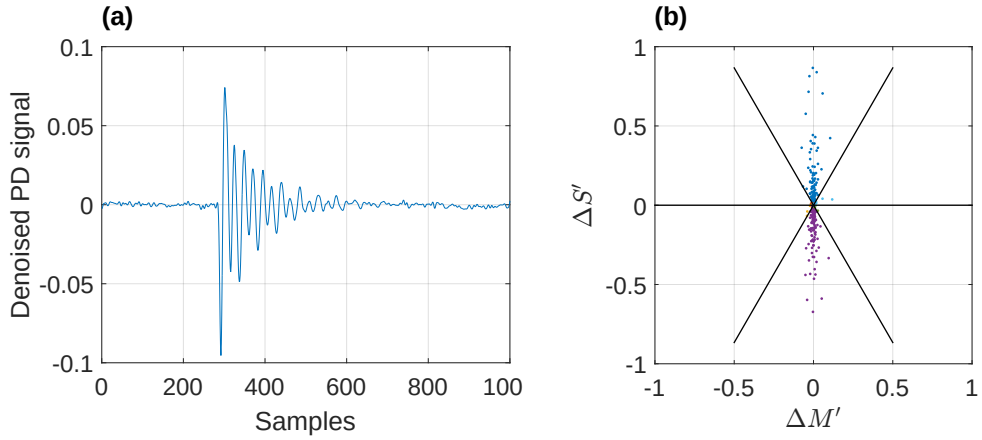

Figure 19. (a) Denoised Partial Discharge pulse, (b) GPT of the Denoised Partial Discharge pulse.

6.2.3. Audible white noise In this last example, a white noise from a acoustic sound recorded by an electronic device was processed. The White noise was downloaded from [43], it was recorded in a study at a sampling rate of 48kHz. The processed signal was chopped at length of 10,000 samples. The time domain signal is plotted in Figure 20 (left) for a zoomed range of samples and its corresponding GPT transformation on the right of the same figure. The eccentricity ϵ and the normalized number of point per pattern is presented in table 4. For this case, a mix of white and pink noise is characterized, by comparing these values with the ones founded in table 3.

The spectrum of its frequency domain presented in Figure 21 shows a monotony spectrum density with a light attenuation at the highest frequencies. This fact can be associated with the pseudo-pink characteristic of this noise revealed by its eccentricity. Further studies should by develop in this case.

With these last three examples in can be shown the potential of GPT to characterize the type of noise that might be present in a given 1D record. Although it is not a rigorous demonstration, it is sufficiently explicit to provide the reader with a tool whose potential application can be very useful. By last, the eccentricity and normalized number

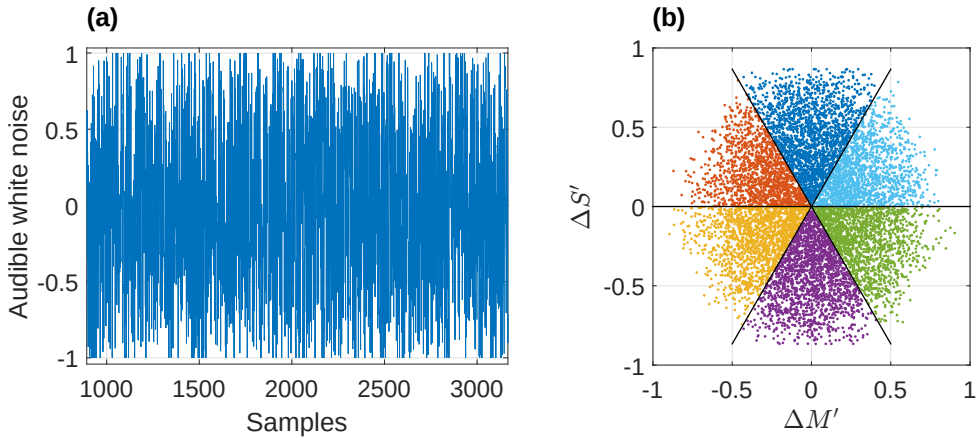

Figure 20. (a) Audible white noise, (b) GPT of the Audible white noise.

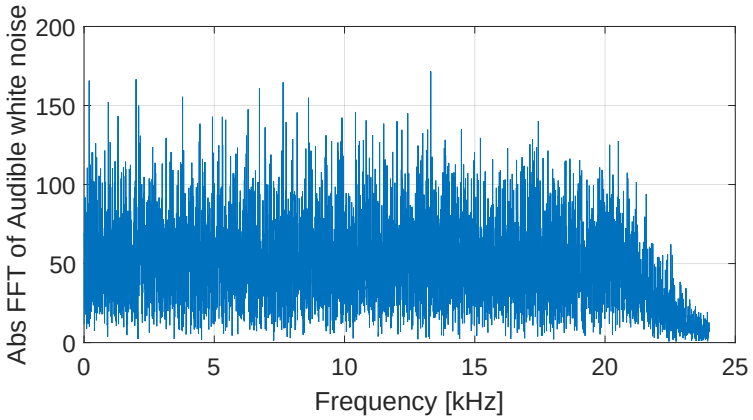

Figure 21. Module of FFT spectrum of audible white noise signal.

of points in each pattern for the three studied cases are presented in table 4. A new column was added to indicate the type of noise assigned base on the calculated eccentricity.

Noise	ϵ	123	132	231	321	312	213	noise type
ECG	+0.7795	0.2376	0.1337	0.1278	0.2396	0.1345	0.1267	pink - red
PD	+0.9090	0.3066	0.1002	0.0972	0.2996	0.1012	0.0952	red
Audible WN	+0.5439	0.2020	0.1445	0.1598	0.1892	0.1556	0.1487	white - pink

Table 4. The values in the six columns on the right correspond to the fraction of GPTs computations that occupied in each pattern by color noise, they are normalized in each row. The eccentricity ϵ is computed according the expression 21 .

7. Final Summary and Conclusions

In the present work, four properties of the GPT have been presented, shown it as a versatile tool for the study and analysis of 1D data series. On the one hand, it can access the representation of the phase space of a dynamic system from a 1D signal without the need to estimate any parameter required by the corresponding algorithms. On the way to reaching the representation in the phase space, the necessary transformations have been obtained to regularize

and normalize the hexagon that contains the GPT image, being an additional result that contributes to analyzing signals independent of their measurement scale or amplitude.

The ability of the GPT to detect the presence of tied data in data series was exposed in this work. The relevance of managing the tied data is of interest but demands a prior efficient algorithm to detect them. In this way, the application of the GPT brings the capability to detect repeated data as well as to analyze signals for other purposes.

The study of the forbidden patterns in chaotic systems has generated different paradigms to interpret it and to model it for later management. The GPT application has been shown in this research to be an overwhelming tool to detect some forbidden pattern. For the particular case exhibited in the section 5, the analytic formulation constitutes a solid confirmation of the absence of the patterns, beyond the numerical results provided by the application of the GPT. Adding to the computational performance of the GPT the possibility of detecting forbidden patterns and its link with chaotic behavior has its intrinsic value.

For the characterization of noise contained in a signal, it is usually analyzed in the Fourier frequency domain or through other transforms such as wavelets. Additionally, a diversity of filters with different technologies are also usually used for this purpose. The use of the GPT in the study of the colored noises of a signal could be not limited to its characterization but also allows comparison of its intensity concerning that of the signal itself. It is also possible to group it within the typologies of known noises to identify the possible source of it. The introduction of the extended concept of eccentricity to a cloud of points in the regions defined by the GPT has shown the applicability of the methodology and contribute to quantify the analysis. The counting of the occupancy of every region of the GPT gives a characteristic of the geometric shape of the signal. Through the examples presented in this work, the ability to characterize the kind of noise in ECG, partial discharge and white sound signals in a clear way without resorting to any of the traditional methodologies has been shown. The computation of the Fourier Transforms was used for a mere confirmation of the results.

It is worth to mention and discuss some limitations of the GPT transform and the scope of the present work. In first place, the symbols generated from an embedding vector of size 3 (y_i, y_{i+1}, y_{i+2}) has been studied, which corresponds with 6 different ordinals patterns perfectly defined in the ΔM and ΔS plane. Further studies are needed to evaluate the mapping obtained from a higher embedding dimension vector, to determinate the new generated symbols and analyze how the ΔM and ΔS plane maps these new patterns. Another aspect that needs to be considered and analyzed is how the sampling frequency modifies the GPT mapping. From a theoretical point of view, given a signal sampled at a sampling rate many times higher than its Nyquist frequency it is expected to have many 123 and 321 patters in the GPT plane since there will to be many samples ascending to a maximum or descending to a minimum. On the other hand, a signal sampled strictly at a sampling rate just above its Nyquist frequency it will be mapped with very few 123 and 321 patterns, since the signal it will be jumping from maxima to minima all the time. Thus, a proper balance it should be found so as the GPT could map relevant features from the signal under analysis. It should also be noted from the expressions presented in the section 2, that it is easy to understand that an on-line implementation requires only two samples behind ($t-1$ and $t-2$) from a certain time (t) to obtain the GPT coordinate, and there is no need of high computer capacity, since the operations to be performed are quite simple. But if the normalization of the GPT is mandatory, no on-line implementation is possible since all samples are needed in order to normalize. In that case, a sliding window with some memory buffer or a batch-processing workflow might be a possible solution, demanding higher processing and data handling requirements.

From a holistic point of view within the flowchart of signal analysis, GPT can contribute in the exploratory analysis of data. On the one hand, it can be used as a study tool to analyze the possible chaotic behavior of a signal of a system by finding in a simple and direct way the characteristic of a forbidden pattern. On the other hand, it allows to reconstruct the phase space in a very simple way and practically without any assumption of the nature of the system that generates the signal, in addition it does not require the determination of any parameter. Furthermore, dealing with repeated data in a clear and unambiguous way can help to analyze the prevalence of states of a system or help to detect the necessity to change the sampling frequency if it is known the presence of tied data is an artifact. After all the studies and examples presented in Section 6, it was shown that the GPT provides a reasonable tool to characterize the signal colored noise, once its presence can be detected by other methodology.

Acknowledgements

The authors would like to thank Eng. Leandro Robles Dávila for his participation in the review of the paper and his valuable contributions in its preparation. The authors would very grateful to Grant Project PID UTN 10125, and PhD. fellowships Program of the Universidad Tecnológica Nacional.

REFERENCES

1. C. Bonini, A. Rey, D. Otero, A. Amadio, M. G. Blesa, and W. Legnani, "An alternative computation of the entropy of 1D signals based on geometric properties," *Statistics, Optimization & Information Computing*, vol. 10, no. 4, pp. 998–1020, 2022.
2. J. M. Amigó, S. Zambrano, and M. A. Sanjuán, "True and false forbidden patterns in deterministic and random dynamics," *Europhysics Letters*, vol. 79, no. 5, p. 50001, 2007.
3. O. A. Rosso, L. C. Carpi, P. M. Saco, M. G. Ravetti, H. A. Larrondo, and A. Plastino, "The Amigó paradigm of forbidden/missing patterns: a detailed analysis," *The European Physical Journal B*, vol. 85, pp. 1–12, 2012.
4. S. S. Soliman and M. D. Srinath, "Continuous and discrete signals and systems," *Englewood Cliffs*, 1990.
5. D. P. Feldman, *Chaos and dynamical systems*, vol. 7. Princeton University Press, 2019.
6. A. Carrión García, *Signal modality characterization: from phase space reconstruction to real applications*. PhD thesis, Universitat Politècnica de València, 2018.
7. B. G. Petty, *Basic electrocardiography*. Springer Nature, 2020.
8. M. U. Maillot and F. M. Pessana, "A new feature space for partial discharge signal separation based on dwt coefficient variance," *Journal of Electrical Engineering*, vol. 6, pp. 18–27, 2018.
9. X.-D. Zhang, *Modern signal processing*. Walter de Gruyter GmbH & Co KG, 2022.
10. C. L. Byrne, *Signal Processing: a mathematical approach*. CRC Press, 2014.
11. C. Bandt and B. Pompe, "Permutation entropy: a natural complexity measure for time series," *Physical review letters*, vol. 88, no. 17, p. 174102, 2002.
12. M. Ribeiro, T. Henriques, L. Castro, A. Souto, L. Antunes, C. Costa-Santos, and A. Teixeira, "The entropy universe," *Entropy*, vol. 23, no. 2, p. 222, 2021.
13. A. Myers and F. A. Khasawneh, "On the automatic parameter selection for permutation entropy," *Chaos: An Interdisciplinary Journal of Nonlinear Science*, vol. 30, no. 3, 2020.
14. M. Riedl, A. Müller, and N. Wessel, "Practical considerations of permutation entropy: A tutorial review," *The European Physical Journal Special Topics*, vol. 222, no. 2, pp. 249–262, 2013.
15. D. A. Lind, D. Lind, and B. Marcus, *An introduction to symbolic dynamics and coding*. Cambridge university press, 2021.
16. Y. Hirata and J. M. Amigó, "A review of symbolic dynamics and symbolic reconstruction of dynamical systems," *Chaos: An Interdisciplinary Journal of Nonlinear Science*, vol. 33, no. 5, 2023.
17. C. Tsallis, "Entropy," *Encyclopedia*, vol. 2, no. 1, pp. 264–300, 2022.
18. M. Obremski and M. Skorski, "Renyi entropy estimation revisited," in *Approximation, Randomization, and Combinatorial Optimization. Algorithms and Techniques-20th International Workshop, APPROX 2017 and 21st International Workshop, RANDOM 2017*, pp. 20–1, Schloss Dagstuhl-Leibniz-Zentrum fur Informatik GmbH, Dagstuhl Publishing, 2017.
19. O. A. Rosso, L. De Micco, H. A. Larrondo, M. T. Martín, and A. Plastino, "Generalized statistical complexity measure," *International Journal of Bifurcation and Chaos*, vol. 20, no. 03, pp. 775–785, 2010.
20. M. Martin, A. Plastino, and O. A. Rosso, "Generalized statistical complexity measures: Geometrical and analytical properties," *Physica A: Statistical Mechanics and its Applications*, vol. 369, no. 2, pp. 439–462, 2006.
21. V. I. Arnol'd, *Mathematical methods of classical mechanics*, vol. 60. Springer Science & Business Media, 2013.
22. V. I. Arnol'd, "Instability of dynamical systems with several degrees of freedom," in *Hamiltonian Dynamical Systems*, pp. 633–637, CRC Press, 2020.
23. M. Golubitsky and I. Stewart, *The symmetry perspective: from equilibrium to chaos in phase space and physical space*, vol. 200. Springer Science & Business Media, 2003.
24. F. A. Mauguière, P. Collins, Z. C. Kramer, B. K. Carpenter, G. S. Ezra, S. C. Farantos, and S. Wiggins, "Roaming: A phase space perspective," *Annual Review of Physical Chemistry*, vol. 68, pp. 499–524, 2017.
25. S. Wiggins, *Chaotic transport in dynamical systems*, vol. 2. Springer Science & Business Media, 2013.
26. J. Amigó, *Permutation complexity in dynamical systems: ordinal patterns, permutation entropy and all that*. Springer Science & Business Media, 2010.
27. J. M. Amigó, L. Kocarev, and J. Szczepanski, "Order patterns and chaos," *Physics Letters A*, vol. 355, no. 1, pp. 27–31, 2006.
28. J. M. Amigó, S. Zambrano, and M. A. Sanjuán, "Combinatorial detection of determinism in noisy time series," *Europhysics Letters*, vol. 83, no. 6, p. 60005, 2008.
29. O. A. Rosso, F. Olivares, L. Zunino, L. De Micco, A. L. Aquino, A. Plastino, and H. A. Larrondo, "Characterization of chaotic maps using the permutation Bandt-Pompe probability distribution," *The European Physical Journal B*, vol. 86, pp. 1–13, 2013.
30. O. A. Rosso, L. C. Carpi, P. M. Saco, M. G. Ravetti, A. Plastino, and H. A. Larrondo, "Causality and the entropy–complexity plane: Robustness and missing ordinal patterns," *Physica A: Statistical Mechanics and its Applications*, vol. 391, no. 1-2, pp. 42–55, 2012.
31. M. R. Roussel, "Maps: stability and bifurcation analysis," in *Nonlinear Dynamics*, 2053-2571, pp. 11–1 to 11–15, Morgan & Claypool Publishers, 2019.
32. A. Kaundanya, A. Anand, K. Raisinghani, and R. Sonkusare, "Analysis of signal noise reduction techniques," in *Proceedings of Third International Conference on Communication, Computing and Electronics Systems: ICCCES 2021*, pp. 425–437, Springer, 2022.
33. R. M. Rangayyan and S. Krishnan, *Biomedical signal analysis*. John Wiley & Sons, 2024.

34. E. Farago, D. MacIsaac, M. Suk, and A. D. Chan, "A review of techniques for surface electromyography signal quality analysis," *IEEE Reviews in Biomedical Engineering*, vol. 16, pp. 472–486, 2022.
35. A. Brandt, *Noise and vibration analysis: signal analysis and experimental procedures*. John Wiley & Sons, 2023.
36. A. Bakulin, I. Silvestrov, and M. Protasov, "Research note: Signal-to-noise ratio computation for challenging land single-sensor seismic data," *Geophysical Prospecting*, vol. 70, no. 3, pp. 629–638, 2022.
37. H. Zhivomirov, "A method for colored noise generation," *Romanian journal of acoustics and vibration*, vol. 15, no. 1, pp. 14–19, 2018.
38. A. Goldberger, L. Amaral, L. Glass, J. Hausdorff, P. C. Ivanov, R. Mark, and H. E. Stanley, "Physiobank, physiotoolkit, and physionet: Components of a new research resource for complex physiologic signals," *PhysioNet*, vol. 101, no. 23, pp. e215—-e220, 2000.
39. G. Luo, D. Zhang, and D. Baleanu, "Wavelet denoising," *Advances in Wavelet Theory and their Applications in Engineering, Physics and Technology*, vol. 634, pp. 6–13, 2012.
40. V. Seena and J. Yomas, "A review on feature extraction and denoising of ECG signal using wavelet transform," in *2014 2nd International Conference on Devices, Circuits and Systems (ICDCS)*, pp. 1–6, IEEE, 2014.
41. "High-voltage test techniques - Partial Discharge measurements," standard, International Electrotechnical Commission, Dec. 2000.
42. C. Bonini, M. U. Maillot, and F. M. Pessana, "Detecting deterioration stages in epoxy resins specimens under partial discharge process," *Journal of Electrical Engineering*, vol. 7, pp. 39–50, 2019.
43. S. Joseph, "Big soundbank - white noise." https://bigsoundbank.com/white-noise-s1037.html. Accessed: 2024-06-05.